J. Fluid Mech. (2007), *vol.* 579, *pp.* 137–161.
doi:10.1017/S0022112007004818 Printed in the United Kingdom

Stability properties of forced wakes

B. THIRIA AND J. E. WESFREID

Physique et Mécanique des Milieux Hétérogènes, Ecole Supérieure de Physique et Chimie Industrielles de Paris (PMMH UMR 7636-CNRS; ESPCI; Paris 6; Paris 7), 10 rue Vauquelin, 75231 Paris Cedex 5, France

(Received 15 November 2005 and in revised form 6 November 2006)

Thiria, Goujon-Durand & Wesfreid (*J. Fluid Mech.* vol. 560, 2006, p. 123), it was shown that vortex shedding from a rotationally oscillating cylinder at moderate Reynolds number can be characterized by the spatial coexistence of two distinct patterns, one of which is related to the forcing frequency in the near wake and the other to a frequency close to the natural one for the unforced case downstream of this locked region. The existence and the modification of these wake characteristics were found to be strongly affected by the frequency and the amplitude of the cylinder oscillation. In this paper, a linear stability analysis of these forced regimes is performed, and shows that the stability characteristics of such flows are governed by a strong mean flow correction which is a function of the oscillation parameters. We also present experiments on the spatial properties of the global mode and on the selection of the vortex shedding frequency as a function of the forcing conditions for $Re = 150$. Finally, we elucidate a diagram of locked and non-locked states, for a large range of frequencies and amplitudes of the oscillation.

1. Introduction

Thiria, Goujon-Durand & Wesfreid (2006) investigated experimentally the flow over a cylinder performing rotary oscillations at moderate Reynolds number. Under forcing conditions, it was observed that vortices were shed at the forcing frequency in the near wake and can merge downstream from each row to give a new pattern similar to the one that can be observed for the unforced case. The wake dynamics was found to be strongly affected by the forcing parameters (the frequency and the amplitude of the cylinder oscillation). The far-wake region exhibits slightly different dynamics of the fluctuations than observed in the free case. Similar observations have been made by Lu & Sato (1996), Chou (1997) and Choi, Choi & Kang (2002) in numerical simulations in the case of a rotary oscillating cylinder, but also in the case of a translating oscillating cylinder as in the experiments performed by Nishihara, Kanedo & Watanabe (2005). However, Thiria *et al.* (2006) were only focusing on the relation between the wake pattern and the drag on the cylinder and none of the other studies on this subject addressed the mechanism responsible for the modification of the wake dynamics.

The stability properties of bluff body wakes have been extensively investigated in recent years. It is well known that when the Reynolds number is bigger than $Re = 47$, the wake of a cylindrical cylinder undergoes self-sustained oscillations; this is the Bénard–von Kàrmàn instability. In this supercritical regime, the properties of these synchronized open flows are strongly dependent on the Reynolds number. Experimentally, the relationship between the Strouhal frequency of the vortex

shedding and the Reynolds number was established long ago by Camichel, Dupin & Teissié-Solier (1927) and Bénard (1928) and more recently by, for example, Provansal, Mathis & Boyer (1987) and Williamson (1988). Goujon-Durand, Jenffer & Wesfreid (1994), Zielinska & Wesfreid (1995) and Wesfreid, Goujon-Durand & Zielinska (1996) investigated the spatial shape of this global structure and established scaling laws for the amplitude and location of the maximum of the global mode for a large range of Reynolds number above the threshold.

From a theoretical point of view, the study of the global dynamics of synchronized spatially developing flows is based on the analysis of the complex local absolute frequency ω_0 which depends on the streamwise coordinate. For normal modes growing proportionally to $e^{-i(\omega_0 t - k_0 x)}$, where ω_0 and k_0 are respectively the complex absolute frequency and complex absolute wavenumber with zero group velocity, if $\mathrm{Im}(\omega_0) = \omega_{0i} > 0$ the flow is said to be locally absolutely unstable (AU); the perturbations grow *in situ* and overrun the whole flow. On the other hand, if $\mathrm{Im}(\omega_0) = \omega_{0i} < 0$, the flow is considered locally convectively unstable (CU); the perturbations are amplified but advected by the oncoming flow. It is now well known that open flows giving rise to self-sustained (or global) oscillations exhibit a finite region of absolute instability near the bluff body and are convectively unstable downstream (for $x > x_{ac}$). The relationship between global wake frequency and local absolute instability is then determinated from local resonance principles. Koch (1985) conjectured that the local resonance responsible for the frequency adopted by the whole flow prevails at the downstream location x_{ac} ($\omega_{ac} = \omega_0(x_{ac})$) while Pierrehumbert (1984) proposed that this resonance is dictated by the local eigenvalue with the maximum imaginary part (located at x^m). More recently, a linear criterion for the selection of global frequencies based on local absolute stability characteristics of the flow has been given by Chomaz, Huerre & Redekopp (1991) and Le Dizes *et al.* (1996). The local frequency prevailing for the whole wake is given by a saddle-point condition based on the analytic continuation of $\omega_0(x)$ in the x-plane given by $\omega_s = \omega_0(x_s)$ with $\mathrm{d}\omega_0/\mathrm{d}x(x_s) = 0$.

These criteria are all based on local properties of the flow, but one can note however that the global frequency can also be calculated by perturbing the whole two-dimensional flow field directly (see for example Barkley, Gomes & Henderson 2002). While these methods can provide very accurate results in open flows, they cannot give local stability properties which are of great importance for the physical understanding of such flows.

1.1. *Stability analysis and forced flow*

Stability analysis requires knowledge of the basic state of the flow being considered. In our case (the cylinder performs rotary oscillations) and more generally for forced systems, the basic flow is modified by the non-stationary characteristics of the forcing.

As was noted by Pier (2002), the linear global frequencies ω_{ac}, ω_{max} and ω_s and ω_{ca} obtained from the *basic* flow analysis cannot account for the real global frequency selected by the wake. From his results (see figure 1), the criterion giving a good frequency prediction for the fully developed vortex street was obtained from a stability analysis applied on the time-*averaged* mean flow instead of the unperturbed basic flow, using the frequency ω_s. This is not the first time that a linear criterion applied to the mean flow has turned out to be the best for the prediction of the actual global frequency in bluff body wakes (see Mattingly & Criminale 1972 or Triantafyllou, Triantafyllou & Chryssostomidis 1986). More recently, Hammond & Redekopp (1997), found in the case of the wake of a blunt-edged plate, that the

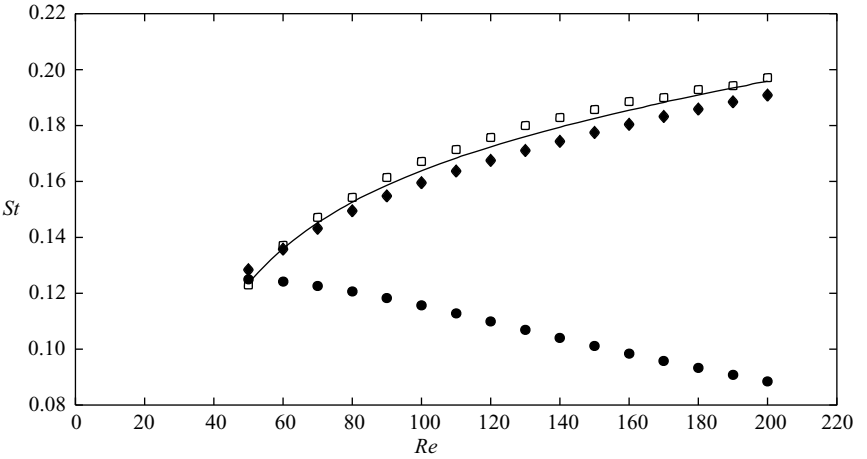

FIGURE 1. Evolution of the global selected frequency in the wake of a circular cylinder as a function of the Reynolds number. □, Frequency obtained by direct numerical simulation (DNS); —, experimental results (from Williamson 1988). Results (ω_s) represented by ◆ have been obtained by applying the linear criterion x_s on the time-averaged mean flow. ●, The same calculation applied to the unperturbed basic flow. From Pier (2002)

saddle-point theory applied to the mean flow provided an accurate prediction of the frequency selected by the system.

But even though the averaged mean flow does not obey the stationary Navier–Stokes equation, it seems that it takes into account the nonlinear mean flow correction and plays the role of a new basic state for the development of linear modes, as was conjectured by Thiria (2005), and discussed in Thiria, Bouchet & Wesfreid (2007*a*) and Barkley (2006). In this paper, we study the mean flow corrections induced by the forcing. Once these mean flow modifications are obtained, a stability analysis of such forced flows will be performed using experimentally measured velocity fields of forced wakes. From this linear stability analysis, we obtain, for the first time, the phase diagram of locked states, and we can establish the boundaries between the regions of global stability and instability. Thus, we contribute to the physical understanding of forced flows and confirm the fundamental role played by the mean flow in the wake stability properties.

2. Experimental set-up

2.1. *Description of the hydrodynamic tunnel and experimental method*

The experiments have been performed in a low-velocity water tunnel with a $10\,\mathrm{cm} \times 10\,\mathrm{cm}$ cross-section. The typical velocity is $3\,\mathrm{cm\,s^{-1}}$ The circular cylinder has a diameter $d = 0.5\,\mathrm{cm}$ which corresponds for our typical velocity U_0 to a Reynolds number $Re = U_0 d/\nu = 150$. This cylinder is mounted on a submerged electrical computer-controlled motor. A detailed description of this set-up can be found in Thiria *et al.* (2006).

The wake visualizations were obtained in the (x, y)-plane using laser induced fluorescence (LIF) (see figure 2). Velocity fields in the near wake $(-1d < x < 8d, -3d < y < 3d)$ in the same (x, y)-plane were obtained using standard particle image velocimetry (PIV) by *LaVision* using a 16×16 interrogation window

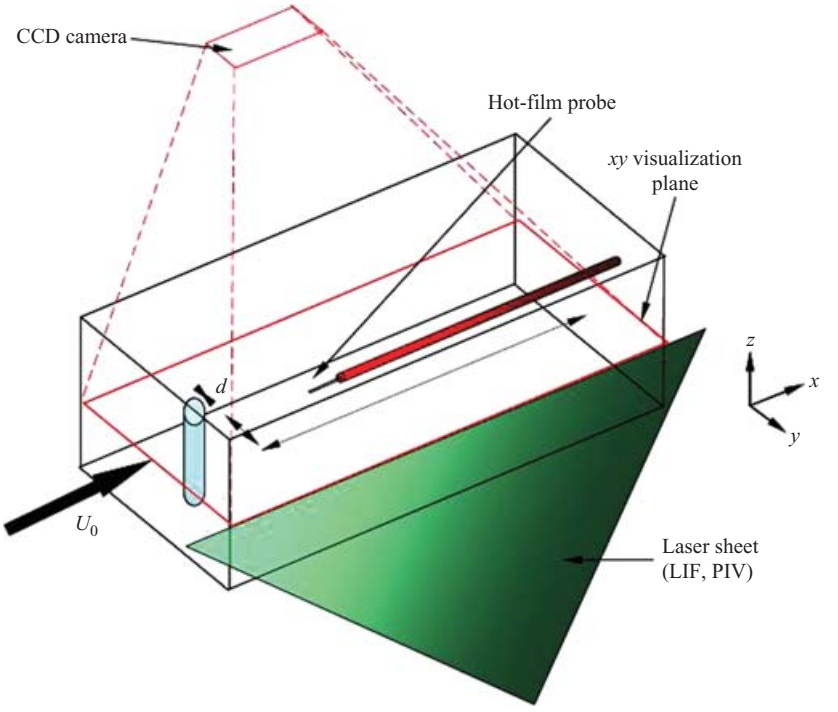

FIGURE 2. Illustration of the hydrodynamic tunnel test section.

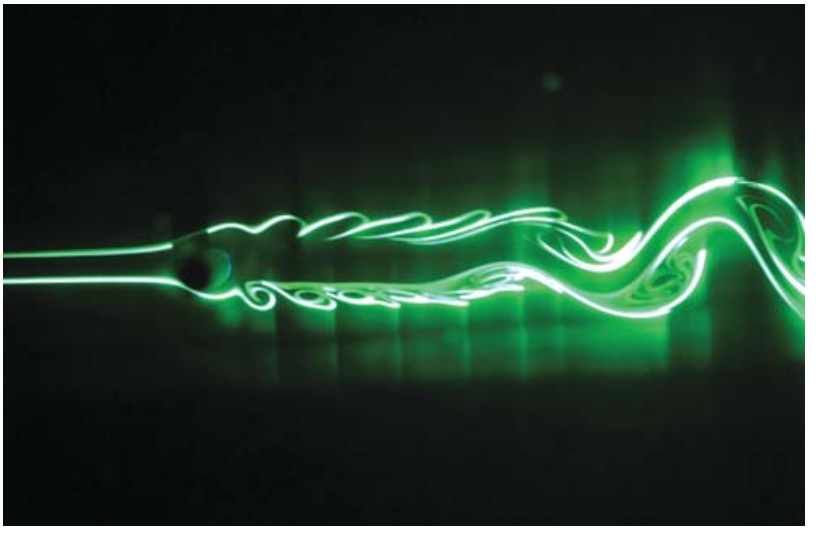

FIGURE 4. Typical flow visualization obtained in the hydrodynamic tunnel under forcing condition $A = 2$, $f_f/f_0 = 4$. The vorticies are shed at the forcing frequency on a characteristic 'lock-in' length in the near wake and merge from each row to give a new pattern similar to that observed for the unforced case.

with an overlap of 50 % which gives a spatial resolution of 22 360 velocity vectors for each field obtained.

In order to get precise measurements of the spectral content of forced wakes, a hot-film probe by *DANTEC* was introduced into the tunnel (figure 2). The probe is

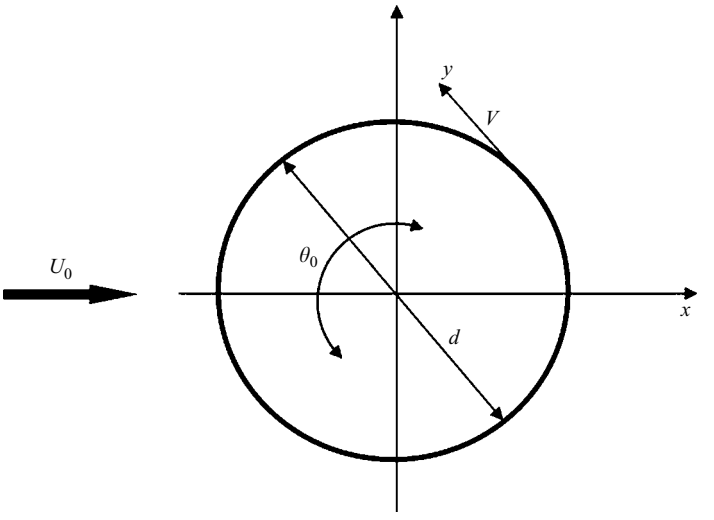

FIGURE 3. Control parameters of the oscillating motion.

free to move in the longitudinal direction x and to different streamwise locations. The hot film is placed in such a way that it measures the velocity modulus in the (x, y)-plane. The evolution of the spectral content can thus be followed as we move downstream of the cylinder. The sampling frequency is 100 Hz which was sufficient for the different dynamics observed.

2.2. *Control parameters*

The cylinder is subjected to oscillations following the law (see figure 3)

$$\theta(t) = \theta_0 \cos(\omega_f t),$$

where ω_f is the angular forcing frequency

$$\omega_f = 2\pi f_f.$$

The forcing amplitude is defined as

$$A = V_{max}/U_0,$$

where $V_{max} = (d/2)\theta_0\omega_f$ is the maximal azimuthal velocity of the forced oscillation. We define f_0 as the global frequency of the unforced wake at the same Reynolds number. There are only two non-dimensional forcing parameters, which are defined by A and the ratio f_f/f_0. An alternative pair of non-dimensional parameters can be used, namely the ratio of the forcing frequencies and the maximal azimuthal displacement s of the cylinder during the oscillation ($s = \frac{1}{2}d\theta_0 = AU_0/\omega_f f_r$). For this Reynolds number, the natural frequency of the vortex shedding measured with the hot film was 0.98 Hz.

3. Forced wake characteristics

We summarize here the global characteristics of the forced flows obtained when the cylinder describes rotary oscillations. A complete experimental study of the different flow regimes and their evolution as a function of the forcing parameters can be found

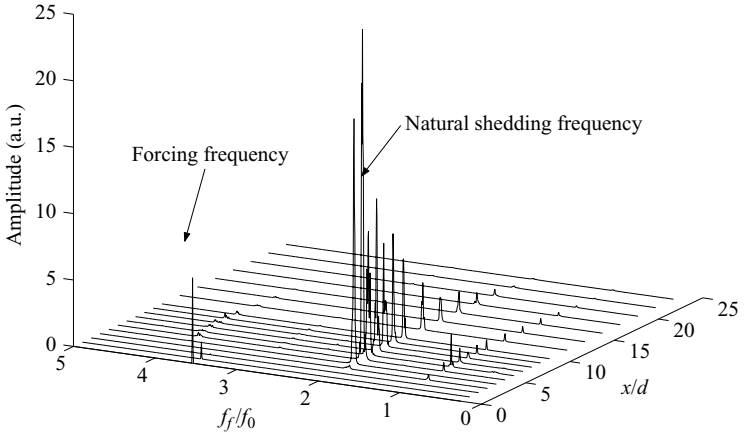

FIGURE 5. Fourier spectra of the velocity fluctuations as a function of the downstream distance from the cylinder. The forcing conditions are $f_f/f_0 = 3.5$, $A = 2$ (non-locked regime).

in Thiria (2005) and Thiria *et al.* (2006)†. As can be seen in figure 4 (see page 140), the forced wake presents a characteristic pattern: the vortices are first shed at the forcing frequency on a characteristic 'lock-in' length in the near wake, which grows with the forcing amplitude A and decreases with the forcing frequency. Downstream from this lock-in region the vortices from each row can merge to give a new pattern similar to the one that can observed for the unforced case. Two different dynamical regimes, which are described in the next section, can be distinguished as a function of the forcing parameters.

3.1. *Spectra*

Figure 5 shows the spatial evolution of the Fourier spectra of the velocity fluctuations, obtained at $y = 0$ as a function of the streamwise coordinate. One can observe that fluctuations coming from the forcing (i.e. in the near wake) decrease quickly. The re-emerging wake exhibits self-sustained oscillations with a sharp front and dissipation downstream. Such typical flow dynamics can be observed for a large range of forcing parameters and the dynamics of the near and far wakes depends strongly on them. This case can be described as *non-locked* (i.e. only a limited part of the wake fluctuations are synchronized with the forcing frequency.). This kind of spectrum corresponds to the streaklines displayed in figure 4. However, one can distinguish another forced regime, which differs from the ones described above. This regime, displayed in figure 6, can be obtained for low forcing frequencies or/and relatively high amplitudes. This case can be considered as a *locked* regime.

As seen in figure 6, the peak related to the forcing frequency decreases quickly in the near wake without any re-emerging pattern and no characteristic far-wake frequency.

Thus, under forcing the wake can behaves in two distinct ways. In § 4, after studying the stability of the forced wakes, we predict their properties as a function of the forcing parameters.

† Movies of streaklines visualizations for each pair of forcing parameters used in that paper ($0.5 < f_f/f_0 < 6$ and $1 < A < 10$) can be found at http://ftp.espci.fr/shadow/thiriaJFM05.

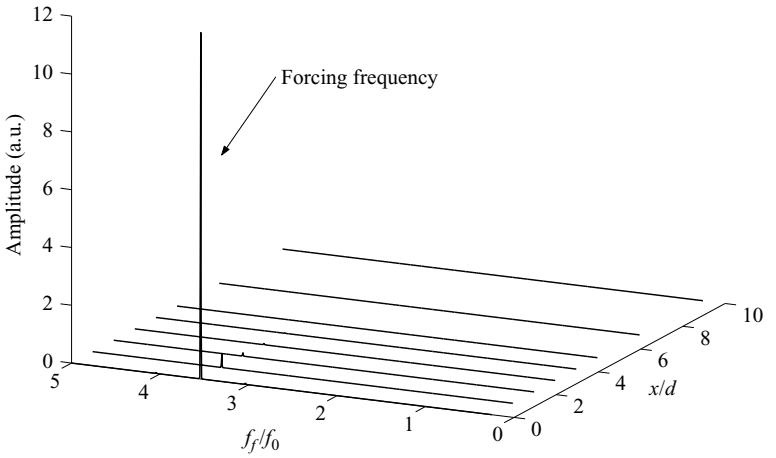

FIGURE 6. Fourier spectra of the velocity fluctuations as a function of the downstream distance from the cylinder. The forcing conditions are $f_f/f_0 = 3.5$, $A = 4$ (locked regime).

3.2. *Mean flow correction*

In previous works, we were interested in the study of the mean (temporally averaged) flow modifications (or the zeroth mode) induced by the presence of fluctuations. For unforced flows, we have studied the spatial distribution of the global mode and also the effect on the recirculation length (Zielinska *et al.* 1997) and the drag (Protas & Wesfreid 2002). In this paper, especially in § 5, we present for the first time, a full experimental study of the evolution of the mean flow as a function of the forcing parameters. The experimental mean fields were obtained by PIV measurements of the near wake of the cylinder using a measurement window between $x = 0$ and $x = 8d$ for different forcing conditions. The mean flow was obtained by averaging 200 instantaneous velocity fields. This number of measured fields, taken at random sampling, was found to be sufficient for the convergence of the averaged field. One of these typical velocity fields is displayed in figure 7 for the unforced case.

4. Stability analysis

In order to understand the local properties of such flows, we performed a stability analysis of the wakes modified by the forcing. Linear stability properties of the measured mean flow were determined by numerical solution of the inviscid Orr–Sommerfeld or Rayleigh equation (see Drazin & Reid 1981) for the streamfunction

$$\Psi(x, y, t) = \int_0^y U(\eta)\,\mathrm{d}\eta + \psi(x, y, t),$$

where $\psi(x, y, t) = \mathrm{Re}\{\phi(y)\mathrm{e}^{\mathrm{i}(kx-\omega t)}\}$:

$$(kU(y) - \omega)(\phi'' - k^2\phi) - kU''(y)\phi = 0, \tag{4.1}$$

with boundary conditions $\phi(-\infty) = \phi(+\infty) = 0$, and where U is the local velocity profile depending on the transverse coordinate y, k and ω are respectively the complex wavenumber and the complex pulsation of the perturbation and ψ is the associated even function.

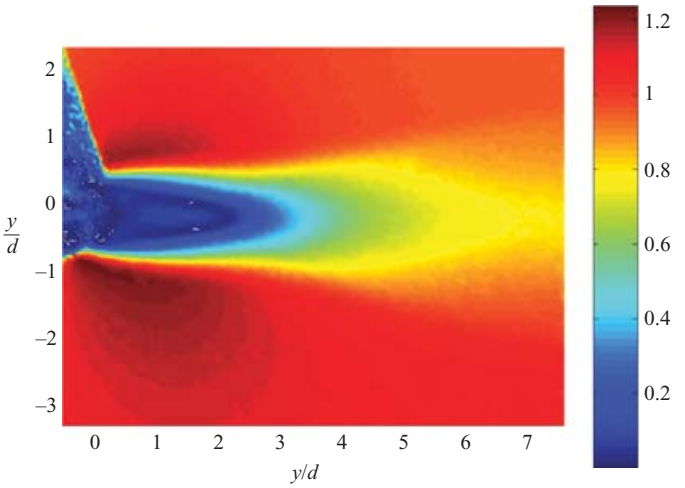

FIGURE 7. Typical velocity field (velocity modulus U/U_0) of the mean flow obtained by PIV for the uncontrolled case at $Re = 150$. In the upper left corner, no velocity can be measured due to the shadow of the cylinder created by the laser sheet.

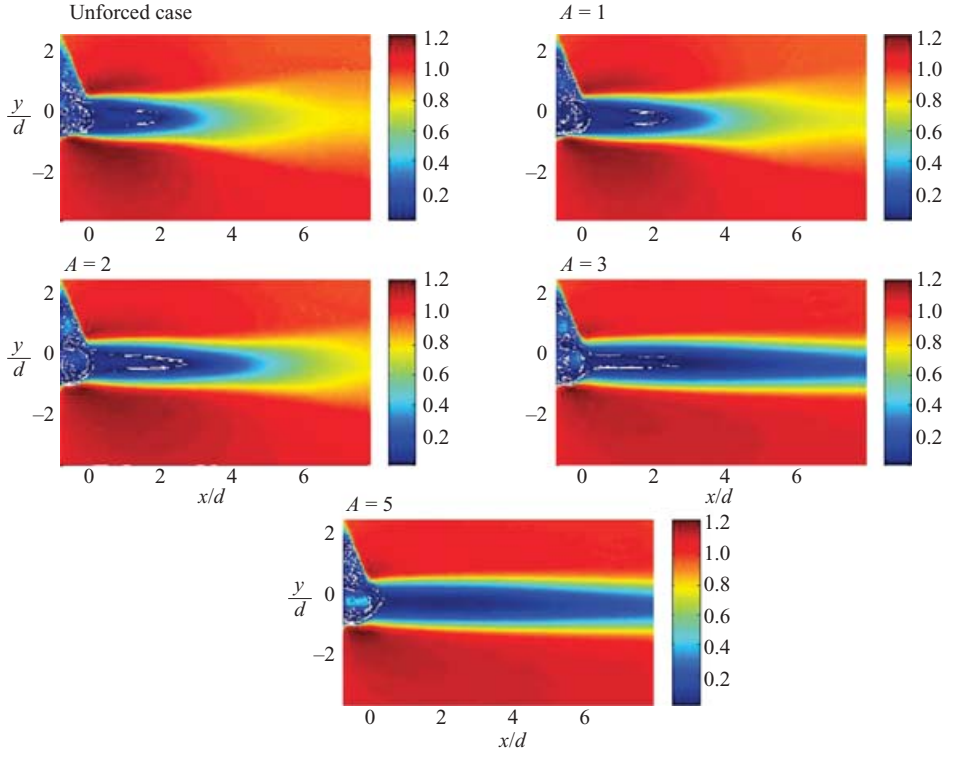

FIGURE 12. Evolution of the mean flow (velocity modulus U/U_0) as a function of the forcing amplitude. The forcing frequency is $f_f/f_0 = 5$.

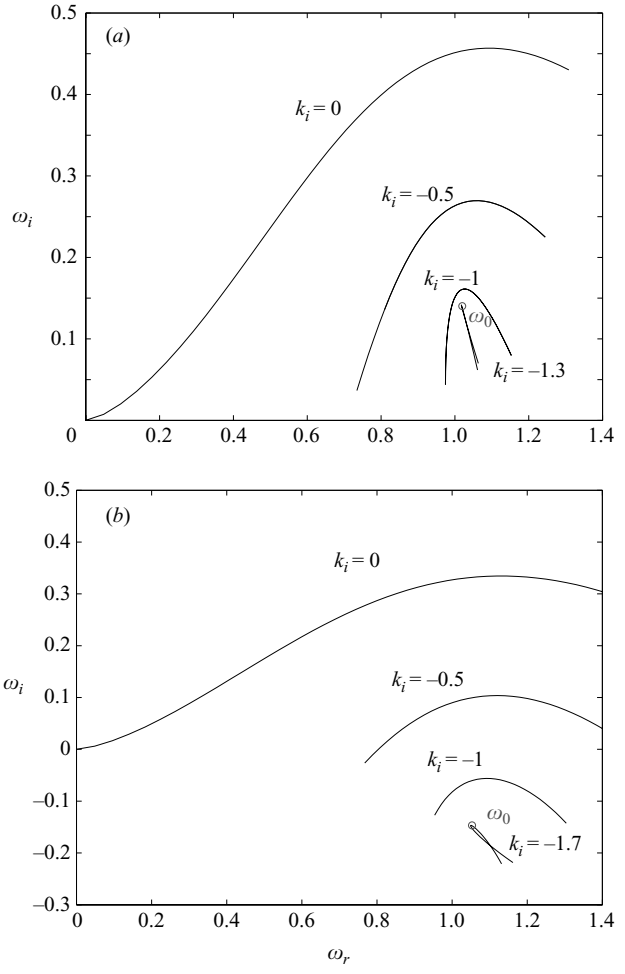

FIGURE 8. Results of the stability calculation for two local profiles at (*a*) $x = 1d$ and (*b*) $x = 2.2d$ taken from the mean flow field displayed in figure 7. The eigenvalue ω_0 is identified at the edge of a cusp-like trajectory. Thus, if the imaginary part of ω_0 lies above the real axis, the flow is said to be locally absolutely unstable while it is said to be locally convectively unstable if $\omega_{0i} < 0$.

Equation (4.1) defines an eigenvalue problem and yields the dispersion relation

$$\mathscr{D}(\omega, k) = 0 \tag{4.2}$$

relating to complex values of ω and k. The absolute frequency ω_0 can be computed where k_0 is specified by requiring the group velocity to vanish:

$$\left(\frac{\partial \omega}{\partial k}\right)_{k_0} = 0. \tag{4.3}$$

The modes are discretized using Chebyshev-collocation points, and a matrix-eigenvalue problem is recovered which is solved numerically for the dispersion relation. The solutions of the eigenvalue were found following the *cusp map procedure* described in Kupfer, Bers & Ram (1987) or Schmid & Henningson (2001). By solving $\omega(k)$, the singularity ω_0 is then identified at the edge of a typical 'cusp'-like trajectory. Thus, if the imaginary part of ω_0 lies above the real axis (figure 8*a*), the flow is said to be

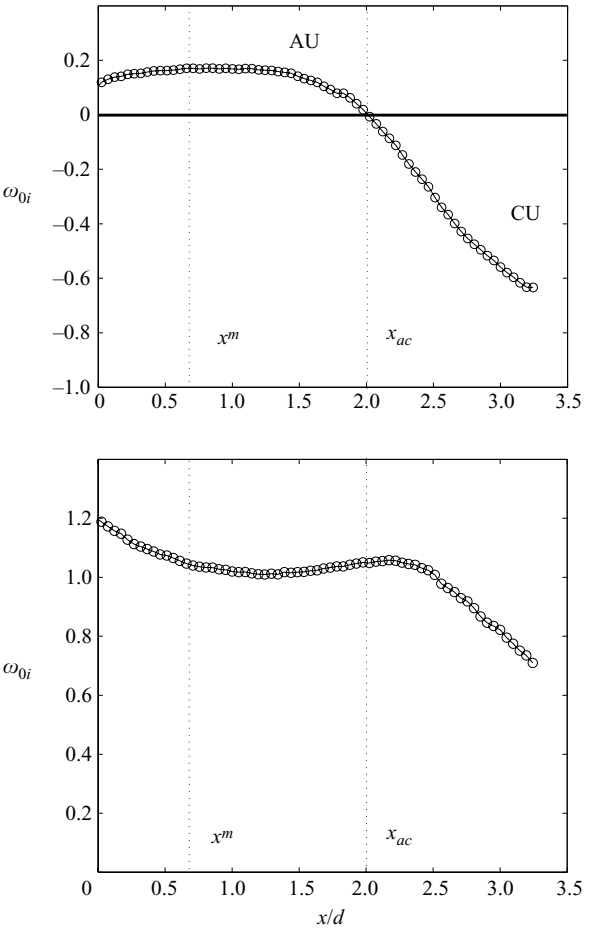

FIGURE 9. Evolution of the imaginary (ω_{0i}) and real part (ω_{0r}) (growth rate and frequency) of the local absolute frequency as a function of the longitudinal coordinate x for the unforced wake at $Re = 150$. The vertical dashed line gives the position x_{ac} (transition from local absolute instability (AU) to local convective instability (CU)) and the localization of x^m (maximum growth rate).

locally absolutely unstable, while it is said to be locally convectively unstable if $\omega_{0i} < 0$ as shown in figure 8(b). We investigated the local stability of the averaged flow as has already been successfully applied to an averaged mean flow by Triantafyllou *et al.* (1986) or Hammond & Redekopp (1997) for the same range of Reynolds numbers.

The procedure is repeated for each profile over the whole explored flow field (from $x = 0$ to $x = 8d$ with step of $\Delta x = 0.05d$). In figure 9, we display the results of this calculation applied to the mean flow of the unforced case (figure 7). This figure shows the imaginary part (absolute growth rate) and real part (absolute frequency) of the non-dimensionalized ω_0 as a function of the x-location. As for each flow fields, $U(x, y)$ has been divided by U_0 and the transverse coordinate y by d, and the relation between ω_{0r} and frequency can be easily determined from the Strouhal number by $\omega_{0r} = 2\pi f_x d/U_0 = 2\pi St$ where f_x indicates the local frequency at location x.

As previously noted, the wake exhibits a finite region of absolute instability ($\omega_{0i} > 0$, for $x < x_{ac} \simeq 2d$) just behind the cylinder, closely following the reverse-flow region

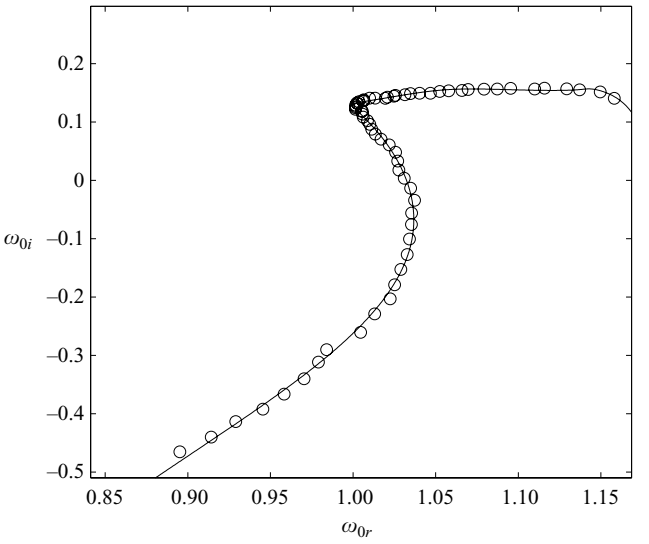

FIGURE 10. Interpolation of the data from figure 9 by a rational function $P^n(x)/Q^n(x)$ with $n = 8$.

$f(x_{ac})$	$f(x^m)$	$f(x_s)$	f_{exp}
1.06 Hz	1.03 Hz	0.97 Hz	0.98 Hz

TABLE 1. Comparison of theoretical predicted linear frequencies with experimental measurements at $Re = 150$.

(cf. figure 7). Farther away, the instability becomes a convective one ($\omega_{0i} < 0$ after $x > x_{ac}$). The results for the absolute growth rate displayed in figure 9 show that the wake is immediately absolutely unstable behind the body and does not exhibit a transition point from convective to absolute instability. The frequency selection criteria discussed in § 1 can be taken into account and compared to the experimental measured frequency. While the ω_{ac} and ω_{max} criteria can be read directly on figure 9, the saddle point criterion requires the analytical continuation of the complex absolute frequencies $\omega_0(x)$ in the complex x-plane. Following Cooper & Crighton (2000), the computed data from the stability calculation displayed in figure 9 have been interpolated by a rational function $P^n(x)/Q^n(x)$, where $P^n(x)$ and $Q^n(x)$ are polynomials of degree at most n (see figure 10). The singularity is removed by varying the imaginary part x_i until a cusp formation corresponding to the point where $\mathrm{d}\omega/\mathrm{d}x = 0$ is verified. Figure 11 displays the localization of the saddle point of the dispersion relation in the complex x-plane, calculated from the experimental mean flow of the unforced case (figure 7).

The different theoretically predicted frequencies (i.e global frequencies obtained at $x = x^m$, $x = x_{ac}$ or $x = x_s$) as well as the real measured global frequency of the wake are summarized in table 1. The three linear criteria give values of the global frequencies close to those measured experimentally. However, the theoretical frequency ω_s given by the saddle-point criterion seems to display better agreement: the predicted frequency is $f(x_s) = 0.97$ Hz while the measured frequency is 0.98 Hz.

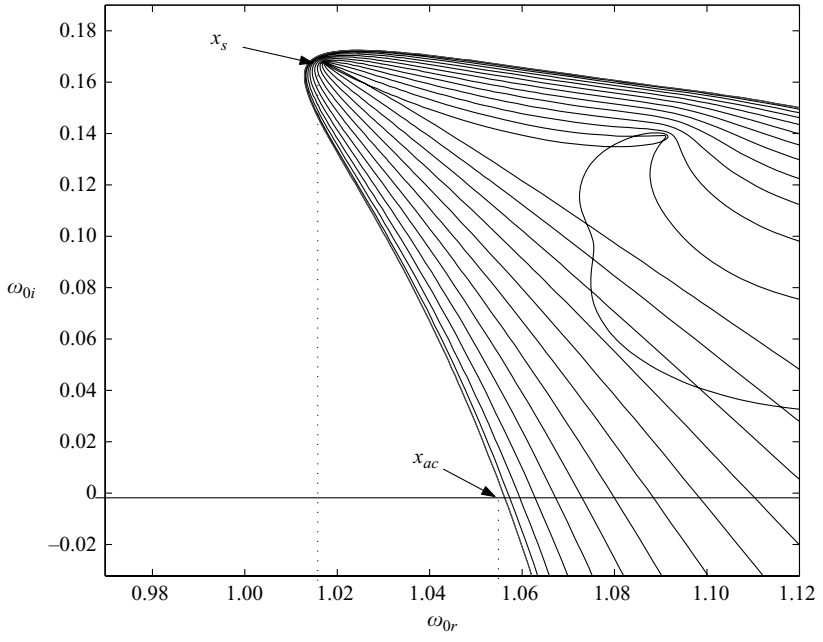

FIGURE 11. Localization of the saddle point of the dispersion relation in the complex x-plane in the unforced case.

This result confirms that the use of an inviscid equation applied to time-averaged mean velocity profiles is sufficient to determine the local properties of the flow as was already observed by Triantafyllou *et al.* (1986) and Hammond & Redekopp (1997); it also confirms that the linear criterion proposed by Chomaz *et al.* (1991) is sufficient to predict the real global frequency from these local characteristics.

5. Mean flow modification and stability properties for forced regimes

We have seen that the stability analysis applied on to unforced case was able to bring out the local and global properties of the wake. Thus, the same procedure will be applied to the same wake under forcing conditions in order to study the modification of these properties as a function of the forcing parameters. We explored the forced regimes in the range of forcing parameters $0 < A < 5$ and $0 < f_f/f_0 < 5$. The forcing frequency $f_f/f_0 = 5$ was found by Thiria *et al.* (2006) to be a regime with minimal drag and where the modifications of the wakes characteristics were significant but varying sufficiently slowly as a function of the forcing amplitude. Thus, this case will be fully detailed first in the following section.

5.1. *Forcing at* $f_f/f_0 = 5$

Figure 12 (see page 144) displays the time-averaged mean flows (velocity modulus as a function of space) for the forcing frequency $f_f/f_0 = 5$ as a function of the forcing amplitude from $A = 0$ (unforced case) to $A = 5$. As can be observed, the mean characteristics of the flow are strongly affected by the forcing conditions. The reverse flow region, initially of length close to two cylinder diameters, starts to grow as we increase the forcing amplitude. When A reaches higher values, the reverse flow region becomes more difficult to detect since negative velocities seem to be absent in the

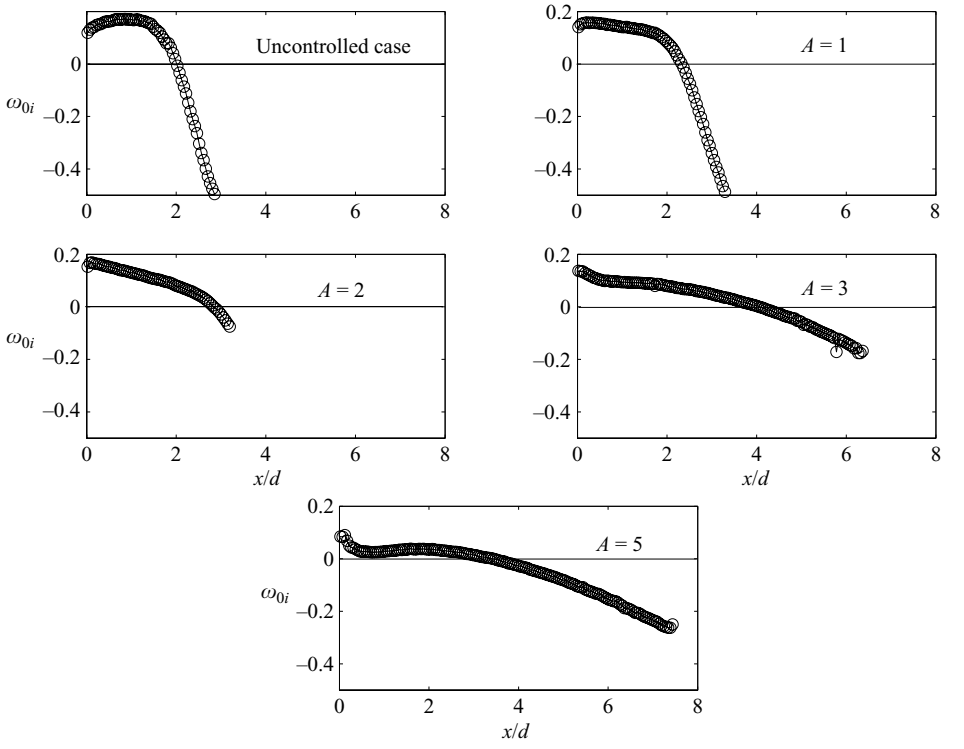

FIGURE 13. Evolution of the spatial distribution of absolute growth rate ω_{0i} as a function of the forcing amplitude at the forcing frequency $f_f/f_0 = 5$. The first curve corresponds to the uncontrolled case displayed in figure 7.

near wake of the cylinder. (Experimental results show that for sufficiently strong forcing amplitude, effectively no negative values of the velocity can be detected. However, recent numerical results (Thiria, Bouchet & Wesfreid 2007*b*) appear to have found such values.) However, this separated region (i.e. region of very weak velocity, compared to the non-wake region) continues to grow. The typical width becomes weaker as the forcing amplitude increases. These measurements confirm the effect of the forcing on the mean flow perturbations, generated through the action of the Reynolds stress.

We extended the stability analysis procedure used for the free case to the averaged mean flows represented in figure 12. In the same way, the real and imaginary parts of the complex local absolute frequency were obtained and both quantities are plotted as a function of the longitudinal coordinate x in figures 13 and 14.

The stability properties of the forced wakes as a function of the amplitude A of the forcing are significantly different. The absolutely unstable region, initially of length two cylinder diameters extends over four diameters for a forcing amplitude $A = 5$. The evolution of this AU region is displayed in figure 15.

For $A = 0$ to 5, the AU region grows gradually spatially and the magnitude of the absolute growth rate globally decreases with the forcing amplitude demonstrating a more stable system. These observations are in agreement with Thiria *et al.* (2006) who observed a strong decrease in the global fluctuation rate for the same forcing configuration. For forcing amplitude $A = 5$, the length of the AU region begins to

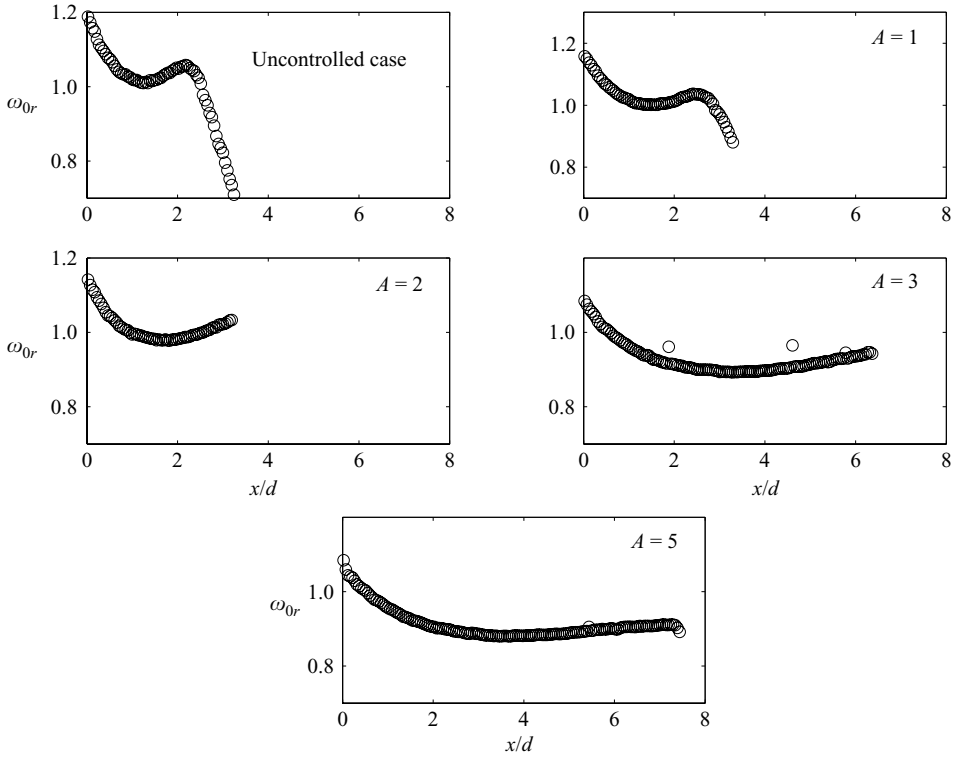

FIGURE 14. Evolution of the spatial distribution of the absolute frequency ω_{0r} as a function of the forcing amplitude, the forcing frequency is $f_f/f_0 = 5$. The first curve corresponds to the uncontrolled case displayed in figure 7.

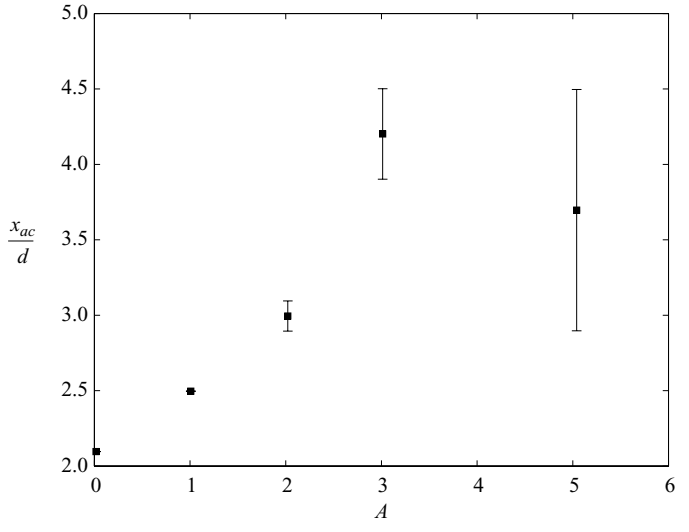

FIGURE 15. Evolution of the absolute unstable region as a function of the forcing amplitude A at the forcing frequency $f_f/f_0 = 5$. The error bars have been determinate graphically from figure 13.

A	0	1	2	3	5
$f_{x_s}(A)$	0.97 Hz	0.95 Hz	0.94 Hz	0.87 Hz	0.85 Hz

TABLE 2. Predicted frequency $f(x_s)$ as a function of the forcing amplitude.

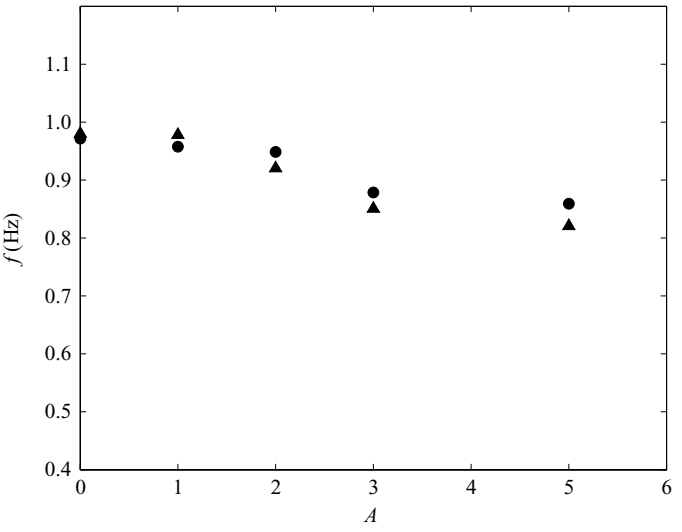

FIGURE 16. Global frequency selected by the wake as a function of the forcing amplitude A for $f_f/f_0 = 5$. ▲, experimental hot-film measurements; ●, theoretical prediction from linear saddle-point criterion ω_s.

reduce. This decrease, which seems to be sign of transition in the instability nature of the wake, will be discussed later as it becomes clearer for the other forcing frequencies.

Nevertheless, for the forcing frequency $f_f/f_0 = 5$, the different cases studied ($0 < A < 5$), all exhibit a finite AU region, characteristic of flows giving rise to self-sustained oscillations. Since the linear stability analysis showed that the forced wakes could give rise to a global mode, one can look for the selected global frequency. In the same way as for the free case, the theoretical global frequency of the forced flows was determinate by looking for the saddle point x_s in the complex x-plane. The results of the computation are displayed in table 2 and plotted in figure 16, to be compared with experimental measurements of the global frequency performed with a hot film, as explained in § 3.1. The theoretical prediction from the linear saddle-point criterion appears to be of great accuracy since the difference between the theoretical and experimental results does not exceed 5 %. The observed tendency is, for both the theoretical and experimental situations, of a slight decrease of the global frequency with the amplitude of the forcing.

Thus, the stability characteristics of these forced wakes are strongly dependent on the forcing amplitude. The cylinder oscillation produces a mean flow correction which is at the origin of the change in the dynamics of the wake. By modifying its *mean* state, the local stability properties are also naturally modified. As a consequence, the system selects a different global mode (thus a different global frequency) related to this new *mean* state. For this forcing frequency, we have seen that the forced wakes always selected a global mode whose characteristics depend on the forcing conditions.

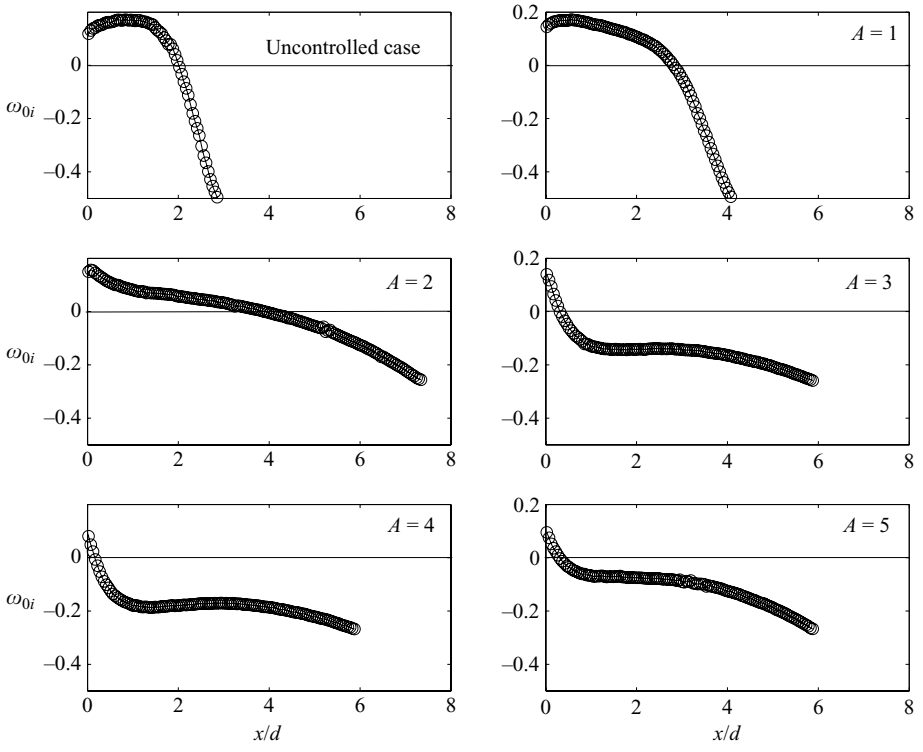

FIGURE 17. Evolution of the absolute growth rate ω_{0i} as a function of the forcing amplitude for a forcing frequency $f_f/f_0 = 4$. The first case corresponds to the uncontrolled flow displayed in figure 7.

5.2. *Forcing at* $f_f/f_0 = 4$

As in the previous section for $f_f/f_0 = 5$, we obtained by PIV measurements the time-averaged mean flows for $f_f/f_0 = 4$ and for A varying from 0 to 5 and used this field as a base for the stability analysis. We discuss here only the results concerning the distribution of the local stability properties of the flow. Figures 17 and 18 display the results of the computation for both the real and imaginary part of the complex absolute frequency ω_0 as a function of the longitudinal coordinate x and the forcing amplitude A.

This case exhibits a similar qualitative behaviour to that previously seen for $f_f/f_0 = 5$. For an amplitude $A = 1$ the typical length of the AU region reaches a value of more than $3.5d$ instead of $2.5d$ for the forcing frequency $f_f/f_0 = 5$ (see figure 15). The predicted saddle-point frequency is lower for a given amplitude than in the results for $f_f/f_0 = 5$. The correction of the mean flow seems to be more important as a function of the forcing amplitude as the forcing frequency is lower.

However, while the flow is able to develop global modes for the range of the amplitude of the oscillation $0 < A \lesssim 3$ (i.e. there exists an AU/CU transition) the cases for higher values of the forcing amplitude exhibit a completely different behaviour.

As can be observed for the cases $f_f/f_0 = 4$, $A > 2$ of figure 17, the quasi-totality of the spatial distribution of the local absolute growth rate ω_{0i} is negative. These flows are *globally linearly stable* and behave just as amplifiers of external disturbances. In addition, the hot-wire measurements confirm that certain forcing conditions launch

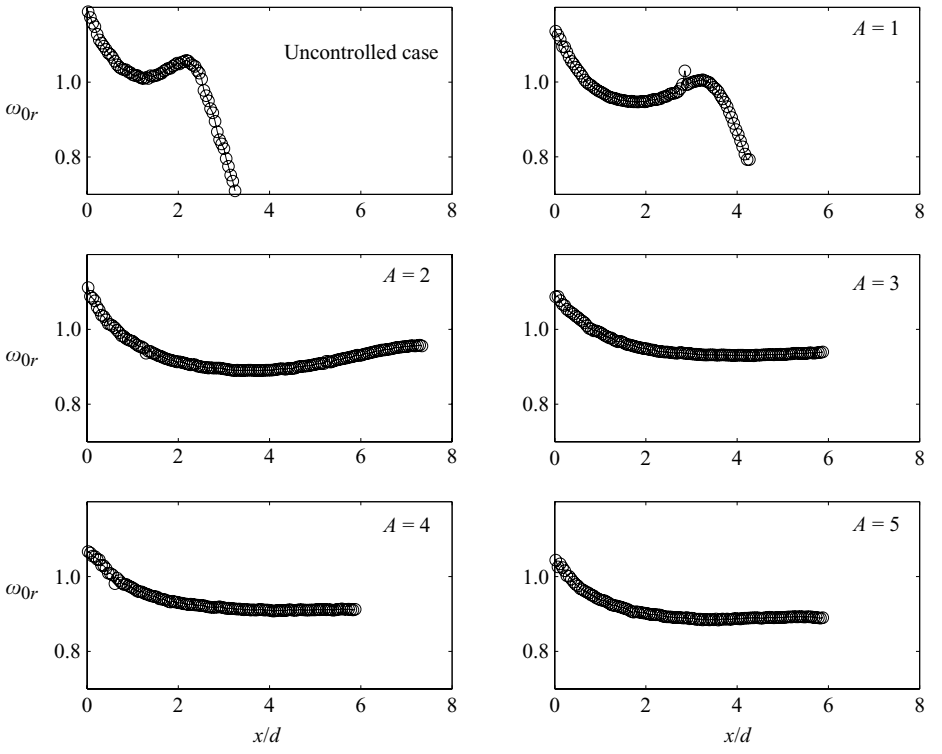

FIGURE 18. Evolution of the absolute pulsation ω_{0r} as a function of the forcing amplitude for a forcing frequency $f_f/f_0 = 4$. The first case corresponds to the uncontrolled flow displayed in figure 7.

this transition from global instability to convective instability (CI). Figure 19 shows two spectra of the fluctuating velocity measured from the axis at the location ($y = 0.5d$) for the two cases of figure 17 outside the lock-in region (i.e where the wake fluctuations do not contain the forcing frequency). The first spectrum has been measured for the forcing conditions $f_f/f_0 = 4$, $A = 2$. The frequency distribution clearly shows the synchronized nature of the flow. The two peaks corresponding to the fundamental mode of the perturbation ($f = 0.98$ Hz) and its first harmonic are characteristic of self-sustained oscillations. These experiments correspond to the theoretical predictions of figure 17. The case $f_f/f_0 = 4$, $A = 4$, taken after absolute/convective transition, exhibits a large band of amplified frequencies as can be observed for convective instabilities. Note that the first peak near $0.8 - 0.9$ Hz can be interpreted as the unstable convective frequency $f(x_s)$ obtained from the linear analysis in the globally stable region (see figure 18).

5.3. *Discussion*

Since the behaviour for the forcing frequency $f_f/f_0 = 4$ was different from that observed for $f_f/f_0 = 5$, we generalized the stability analysis for other forcing frequencies $f_f/f_0 = 3, 2, 1, 0.5$ as a function of the forcing amplitude A. The results of the stability analysis in the $(A, f_f/f_0)$-plane are summarized in figure 20: the circles (●) denote a globally stable flow, while the stars (⋆) denote a globally unstable flow (i.e. a flow supporting a global mode). The lozenges (◇) indicate the transition between these two states.

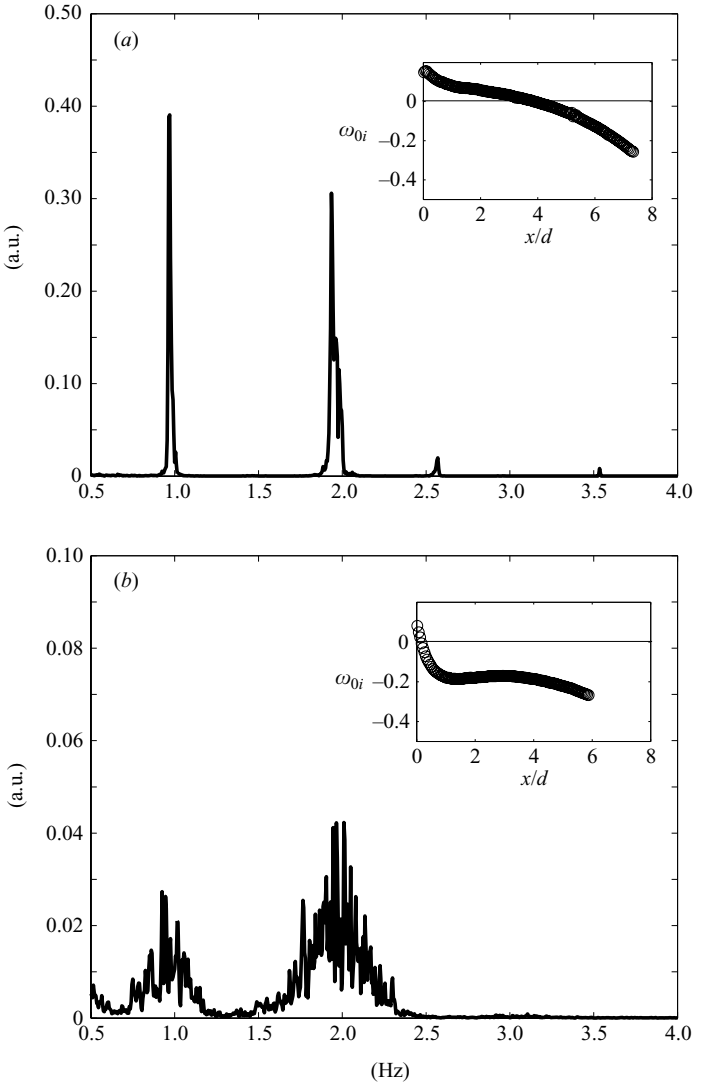

FIGURE 19. Frequency spectra obtained by hot-film measurements outside the lock-in region (i.e. where the wake fluctuations do not contain the forcing frequency): (*a*) $f/f_0 = 4$, $A = 2$, (*b*) $f/f_0 = 4$, $A = 4$.

The lower the forcing frequency, the sooner the transition from global instability to convective instability occurs, except in the subharmonic forcing case where the transition point starts to grow again with the forcing amplitude. For the forcing frequency $f_f/f_0 = 1$, the flow is globally stable as soon as the cylinder begins its motion. This point has not been verified, but with regard to the evolution of the transition point as a function of the forcing frequency, we concluded that the transition GI/GS (global stability to instability) takes place closer to $A = 0$ than to $A = 1$. Nevertheless, the error bars in figure 20 testify to the uncertainly of this transition detection. According to these results, the existence of a global mode in open flows under forcing conditions in the supercritical regime is not intrinsic and depends directly on the forcing parameters.

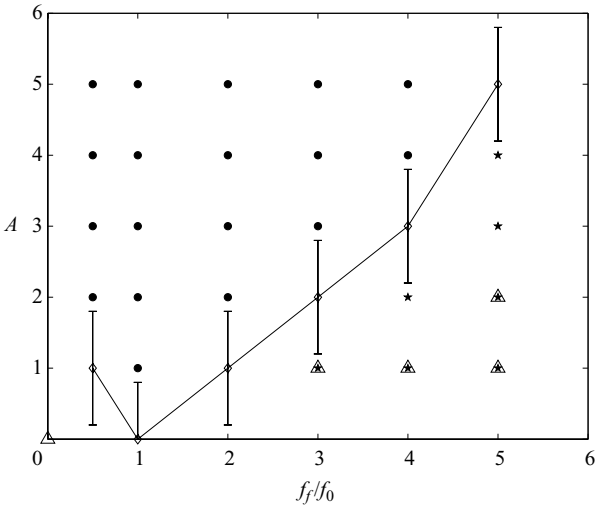

FIGURE 20. Predicted global stability properties of forced wakes in the $(A, f_f/f_0)$-plane: ●, globally stable flow; ⋆, globally unstable flow; ◇, the transition between these two states, corresponding to a critical value of the forcing amplitude A_c, for each forcing frequency. In the globally unstable region, the symbols enclosed by △ correspond to the forcing cases on which a study of the spatial structure of the global mode have been performed.

It is important to note that the boundary between global and convective instability displayed in figure 20 closely follows the curve delimiting the 'lock-on' and 'no lock-on' states in earlier works concerning the behaviour of the lift fluctuations of a circular cylinder in oscillation. Baek & Sung (2000), Baek, Lee & Sung (2001) and Cheng, Chew & Luo (2001), in a similar configuration to the one in this paper, established precisely numerically the two different regimes existing for the wake under forcing conditions. These curve shows a continuous behaviour. The 'lock-on' state describes lift fluctuations (i.e. the footprint of all the fluctuations in the wake, (see Saffman 1992 or Protas & Wesfreid 2003), containing only the forcing frequency. Conversely, the 'no lock-on' state indicates a more complex frequency content that includes the forcing frequency and a frequency linked to the far-wake instability. While the boundary between 'lock-on' and 'no lock-on' was well defined in previous works, the physical mechanisms responsible for this transition are not clear. According to our results obtained from a stability analysis of the mean forced flow, this behaviour can now be fully interpreted from the transition exhibited in figure 20. When the forced wake supports a global mode, a second characteristic frequency emerges and the flow can be described as 'no lock-on'. The 'lock-on' state is reached for forcing parameters that trigger the transition to convective instability. Since no precise frequency due to the wake instability can be observed, only the forcing frequency clearly appears in the frequency spectrum.

This is an important result, which explains the locking diagram in terms of stability properties. The details of the transition displayed in figure 20 will be discussed in detail in a forthcoming paper.

Nevertheless, the properties of these global modes, when they exist, are now defined and are determined by the mean flow correction. The spatial structure of these modes and its evolution as a function of the forcing parameters are developed in the next section.

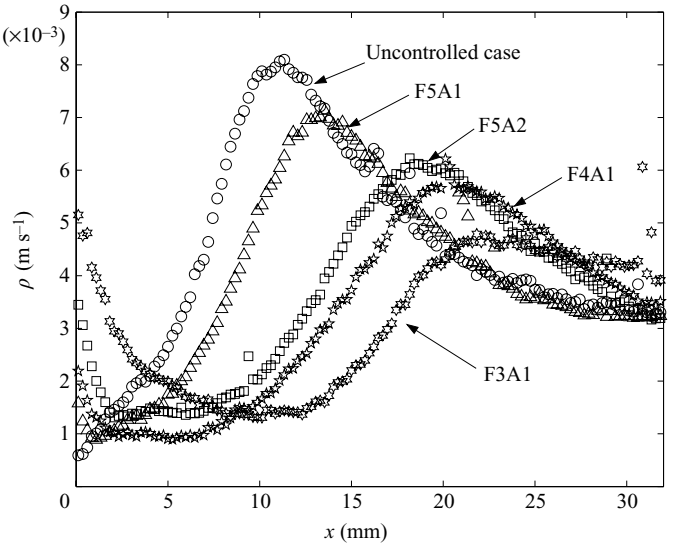

FIGURE 21. Shape of the global mode for the different forcing conditions $f_f/f_0 = 5$, $A = 1$; $f_f/f_0 = 5$, $A = 2$; $f_f/f_0 = 4$, $A = 1$ and $f_f/f_0 = 3$, $A = 1$ at $Re = 150$. The case with no forcing has been added. These values were obtained by measuring the peak to peak value of the fluctuating part of the x component of the velocity, at $y = d$. These forced cases correspond to the points denoted by ($\triangle$) in figure 20.

6. Global mode structure

It is known that in bluff body wakes, the spatial envelope of the coherent oscillation described here is strongly inhomogeneous. The form of the global modes and their dependence on the Reynolds number were investigated by Goujon-Durand *et al.* (1994) and Zielinska & Wesfreid (1995) for triangular bodies and by Wesfreid *et al.* (1996) for circular bodies. They found that the maximum amplitude ρ_{max} of the oscillation as well as the correlation length x_{max} (i.e. the longitudinal position corresponding to ρ_{max}) followed scaling laws above the threshold as in other hydrodynamical instabilities (Wesfreid *et al.* 1978). The amplitude and the position of the *maximum* of these modes then scale as

$$\rho_{max} \sim (Re - Re_c)^{1/2}, \tag{6.1}$$

$$x_{max} \sim (Re - Re_c)^{-1/2}. \tag{6.2}$$

The global-mode form, as well as the scaling laws, are described by a Ginzburg–Landau model (see Chomaz 2005). (This spatial downstream envelope is sometimes described as the perturbation eigenfunction in the flow direction.)

The flow behind a circular cylinder is distorted by a strong nonlinear mean flow correction generated by the presence of fluctuations in the wake. The reverse-flow region, which is a footprint of the mean flow and which initially grows linearly with Re in the subcritical regime, starts to decrease, particularly as $(Re - Re_c)$ increases above the threshold (see Zielinska *et al.* 1997). This distortion changes with the intensity of the quadratic Reynolds stress of the fluctuations.

6.1. *Spatial structure of global modes in forced regimes*

The shape of the global modes, corresponding to the uncontrolled case (or free case) and the forced cases $f_f/f_0 = 5$, $A = 1$; $f_f/f_0 = 5$, $A = 2$; $f_f/f_0 = 4$, $A = 1$ and $f_f/f_0 = 3$, $A = 1$, is displayed in figure 21; the corresponding mean flows are shown

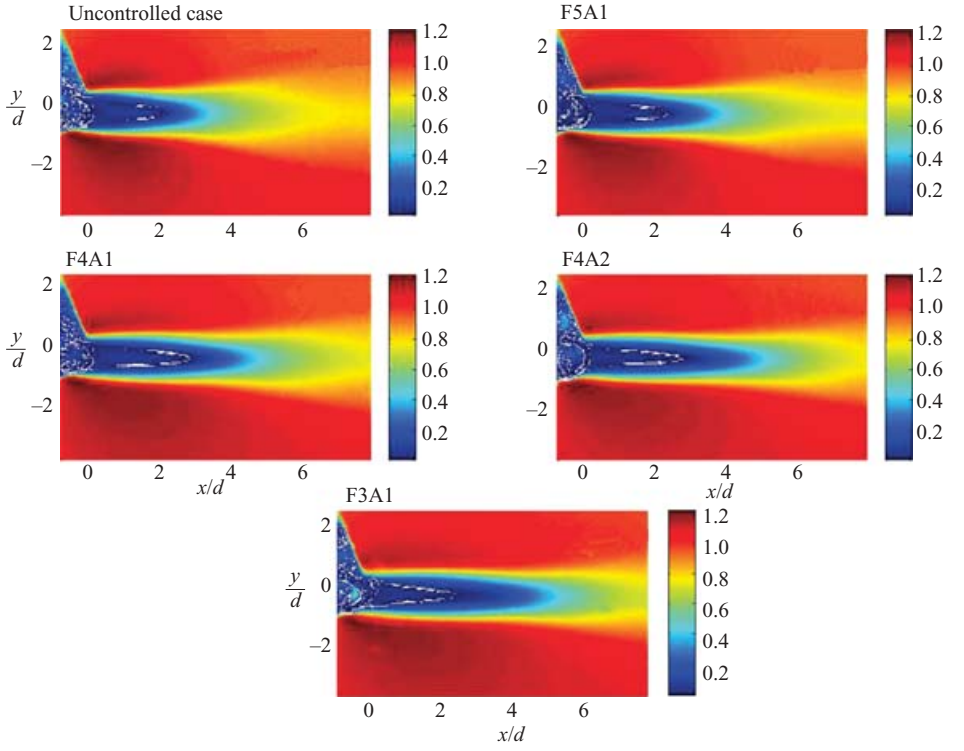

FIGURE 22. Mean flows corresponding to the envelopes displayed in figure 21. As can be seen, the reverse-flow region grows as the magnitude of the instability decreases, showing that the flow tends to return to its basic state.

in figure 22. As we explained in § 2, the mean spatial structures are obtained from PIV measurements computing the r.m.s. fields from 200 instantaneous velocity fields for each forcing condition.

As done by Wesfreid *et al.* (1996) for natural vortex shedding, the global mode shapes, or fluctuation envelopes, were obtained from measurements of the peak to peak value of the longitudinal x component of the fluctuating velocity as a function of the longitudinal coordinate, taken at $y = y_{max}$ (i.e. the position of the maximum of fluctuation v_x). The value of y_{max} was found to be nearly constant as a function of the forcing parameters and equal to d.

The global mode shape characteristics are strongly dependent on the forcing parameters. The closer to the transition GS/GI the forced flow is (i.e. to the neutral (or critical) curve of figure 20), the greater the decrease of the amplitude of the global mode and the further the front of this shape is pushed downstream. This important observation gives an indication that an effective control parameter (and a correlated growth rate) of instability decreases approaching this line. According to our previous work, each global mode shape was renormalized by its maximum amplitude ρ_{max} and its corresponding longitudinal position in the wake x_{max}. This is plotted in figure 23 and we can observe that the normalized shapes can be considered self-similar, suggesting that scaling laws also exist for forced global modes in the same way as for natural wakes. Indeed, we can consider that the growth rate of the global instability changes with the forcing via the modification of the mean flow. (In

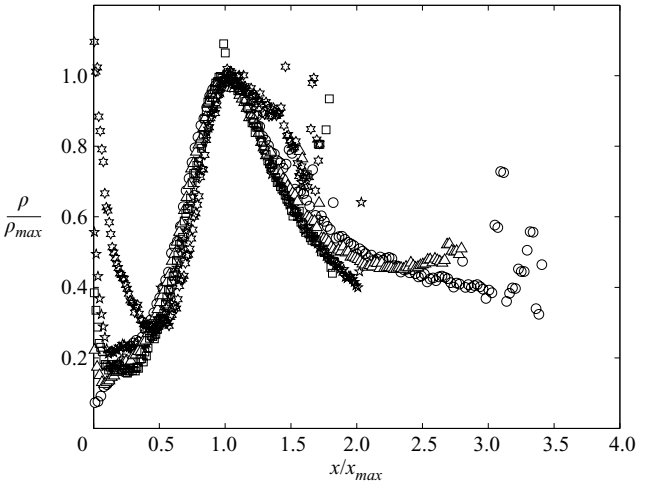

FIGURE 23. Shape of the global modes displayed in figure 21 renormalized by ρ_{max} and x_{max}.

a recent numerical work Thiria *et al.* (2007*b*) showed that, in the same framework (a cylinder performing rotary oscillations at $Re = 150$), $\rho_{max} \sim 1/x_{max}$, as in natural wakes.)

On the other hand, it is clear from figure 23, that this analysis only applies to the wake envelope representing the global mode. This analysis excludes the amplitude of the near wake, which is the footprint of the flapping due to the oscillating cylinder. Indeed, the fluctuations follow the boundary conditions $V_x(x = 0) = V_p$ and $V_x(\rightarrow \infty) = 0$, where V_p is proportional to the forcing amplitude. We concentrated our study on the cases below the critical curve delimitating the lock – on/no – lock – on transition showed in figure 20 (i.e. where a global mode exists).

Note that not all the cases previously analysed were used to study the scaling of the spatial modes. This is due to the high spatial resolution of the experimental fields required for the stability analysis, which, for strong forcing, makes the localization of the global mode shape maximum outside the measurement window impossible.

Finally, it appears that the selection of a global mode for flow under forcing conditions is of the same nature as those selected in the natural case. The difference is that the bifurcation is not triggered by the same control parameter. For greater clarity, this principle is illustrated in figure 24. The length of the reverse-flow region L_r, which is the footprint of the mean state, is plotted as a function of the Reynolds number. In the classic case of the flow behind an obstacle, which can be followed from left to right in figure 24, L_r grows linearly with Re in the stable region, located on the left of Re_c. When $Re > Re_c$, the flow becomes unstable, L_r decreases as a consequence of the mean flow modification (Zielinska *et al.* 1997), and a global mode is selected. Its frequency is then determined linearly by its mean state and its spatial properties are dictated by the scaling laws given in relations (6.1) and (6.2). Under forcing conditions, the mean flow is corrected, the new state then selects a new mode and the bifurcation can be seen this time from up to down. The different forced states with global instability (or no – lock – on state) are distributed on a vertical line (for $Re > Re_c$).

7. Discussion and conclusion

We have seen that a complete linear stability analysis in the parallel approximation applied to mean averaged measured flows can account for the stability properties of

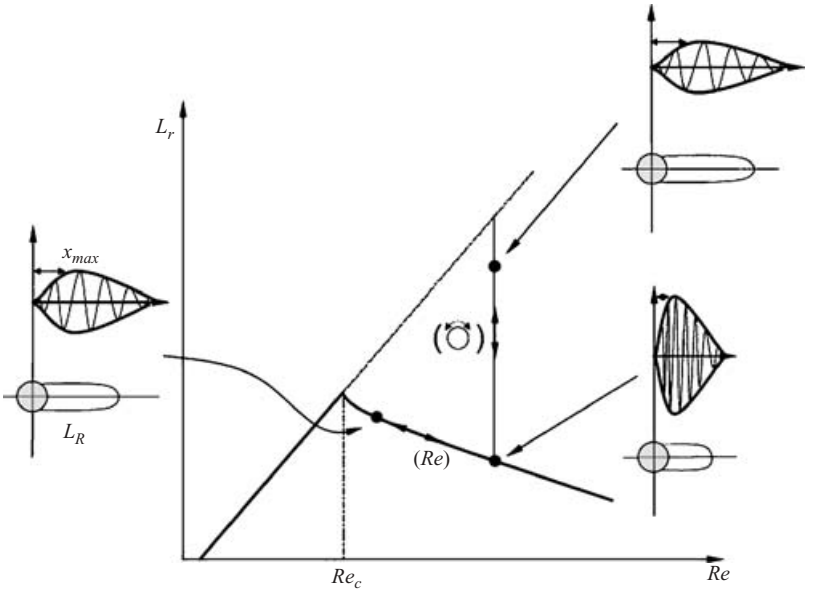

FIGURE 24. Illustration of the possible bifurcations which can occur for a cylinder under forcing conditions. The vertical line, for $Re > Re_c$ is explored when the forcing A goes from 0 (lower branch) to the critical value A_c given by the transition line displayed in figure 20.

wakes under forcing conditions. Until now, the fact that the mean state contains all the flow properties had not been fully established. Our results point clarified this and suggest strongly that the mean flow is the flow that should be considered to give a good description of such complex systems. By adopting the point of view that this modified mean flow plays the role of a new basic state, a linear stability analysis then becomes a powerful tool since it is now possible to understand the dynamic of forced wakes.

Amplitude equations such as the Ginzburg–Landau or Stuart–Landau models which give a good description of the wake dynamics near the threshold could be extended to forced wakes by taking into account the mean flow correction induced by the forcing. Corrections to those models had been already studied in other physical situations such as for the Rayleigh–Bénard instability by Siggia & Zippelius (1981) and Zippelius & Siggia (1983). They introduced an additional term in the Ginzburg–Landau equation due to the existence of a stationary mode generated by a nearly uniform lateral velocity induced by the curvature of the rolls destabilizing the pattern further via the three-dimensional vorticity. This correction was recently introduced in studies of wakes by Noack *et al.* (2003) in order to modify the POD models by coupling the typical Landau model to a second equation for the zeroth mode.
Thus, in order to incorporate the modification of the growth rate due to the forcing, a system of coupled equations can be written in the following form:

$$\left.\begin{aligned} \frac{\mathrm{d}a}{\mathrm{d}t} &= (\gamma + \mathrm{i}\omega_I)a - (c_r + \mathrm{i}c_i)|a|^2 a + (\beta_r + \mathrm{i}\beta_i)ab, \\ \frac{\mathrm{d}b}{\mathrm{d}t} &= -\sigma b + F(|a|^2, A, f_f), \end{aligned}\right\} \tag{7.1}$$

where a is here the complex amplitude of the perturbation and γ, ω_I, c_i, c_r and σ are real coefficients; ω_I would then be the linear frequency selected at the critical

state and which would be *a priori* dependent on the critical forcing parameters (i.e. parameters corresponding to the critical line GI/GS displayed in figure 20).

The equation for b is that of the mean flow correction generated by the forcing, here depending on the variation of the square of the perturbation amplitude between the controlled and uncontrolled case and the forcing parameters, with $F = 0$ when $A = f_f = 0$. This equation is coupled to those used for the free wake (see for example Provansal *et al.* 1987), and so a new term $(\beta_r + \mathrm{i}\beta_i)ab$ appears, which is proportional to $|a^2|a$ in the fully developed case and which modifies the linear growth rate. Such a system could, *a priori*, account for the wake dynamics of a cylinder performing rotary oscillation, which is consistent with our experimental results, and more generally for forced open flows. The consequences of these conjectures will be developed in future studies.

We would like to thank D. Pradal, S. Goujon-Durand and M. de St-Aubert for their assistance concerning the experimental set-up. We acknowledge D. Barkley and L. Tuckermann for fruitful discussions, and B. Protas and B. Pier for providing the numerical data needed for this paper.

This work was supported by Schlumberger in Clamart, France.

REFERENCES

Baek, S.-J., Lee, S. B. & Sung, H. J. 2001 Response of a circular cylinder wake to superharmonic excitation. *J. Fluid Mech.* **442**, 67–88.

Baek, S.-J. & Sung, H. J. 2000 Quasi-periodicity in the wake of a rotationnally oscillating cylinder. *J. Fluid Mech.* **408**, 275–300.

Barkley, D. 2006 Linear analysis of the cylinder wake mean flow. *Europhys. Lett.* **75**, 750–756.

Barkley, D., Gomes, M. G. M. & Henderson, R. D. 2002 Three dimensional instability in flow over a backward-facing step. *J. Fluid Mech.* **473**, 167–190.

Bénard, H. 1928 Sur les tourbillons alternés et la loi de similitude. *C. R. Acad. Sci.* **187**, 1123–1125.

Camichel, C., Dupin, P. & Teissié-Solier, M. 1927 Sur l'application de la loi de similitude aux période de formation des tourbillons alternés de Bénard-Kàrmàn. *C. R. Acad. Sci.* **185**, 1556–1559.

Cheng, M., Chew, Y. T. & Luo, S. C. 2001 Numerical investigation of a rotationally oscillating cylinder in mean flow. *J. Fluids Struct.* **15**, 981–1007.

Choi, S., Choi, H. & Kang, S. 2002 Characteristics of flow over a rotationally oscillating cylinder at low Reynolds number. *Phys. Fluids* **14**, 2767–2777.

Chomaz, J.-M. 2005 Global instabilities in spatially developing flows. *Annu. Rev. Fluid. Mech.* **37**, 357–392.

Chomaz, J.-M., Huerre, P. & Redekopp, L. 1991 A frequency selection criterion in spatially developing flows. *Stud. Appl. Maths* **84**, 119–144.

Chou, M.-H. 1997 Synchronization of vortex shedding from a cylinder under rotary oscillation. *Comput Fluids.* **26**, 755–774.

Cooper, A. J. & Crighton, D. G. 2000 Global modes and superdirective acoustic radiation in low-speed axisymmetrics jets. *Eur. J. Mech.* B/Fluids **19**, 559–574.

Drazin, P. G. & Reid, W. H. 1981 *Hydrodynamic Stabilities.* Cambridge University Press.

Goujon-Durand S., Jenffer, P. & Wesfreid, J. E. 1994 Downstream evolution of the Bénard-Von Karman instability. *Phys. Rev.* E **50**, 308–313.

Hammond, D. & Redekopp, L. 1997 Global dynamics of symmetric and asymmetric wakes. *J. Fluid Mech.* **331**, 231–260.

Koch, W. 1985 Local instability charcteristics and frequency determination on self-exited wake flows. *J. Sound Vib.* **99**, 53–83.

Kupfer, K., Bers, A. & Ram, A. K. 1987 The cusp map in the complex-frequency plane for absolute instabilities. *Phys. Fluids* **30**, 3075–3082.

Le Dizes, S., Huerre, P., Chomaz, J.-M. & Monkewitz, P. 1996 Linear global modes in spatially develloping media. *Phil. Trans. R. Soc. Lond.* A **354**, 169–212.

Lu, X.-Y. & Sato, J. 1996 A numerical study of flow past a rotationally oscillating circular cylinder. *J. Fluids Struct.* **10**, 829–849.

Mattingly, G. & Criminale, W. 1972 The stability of an incompressible two-dimensional wake. *J. Fluid Mech.* **51**, 233–272.

Nishihara, T., Kanedo, S. & Watanabe, T. 2005 Characteristics of fluid dynamic forces acting on a circular cylinder oscillating in the streamwise direction and its wake patterns. *J. Fluids Struct.* **20**, 505–518.

Noack, B., Afanasiev, K., Morzynski, M., Tadmor, G. & Thiele, F. 2003 A hierarchy of low dimensional models for the transient and post-transient cylinder wake. *J. Fluid Mech.* **497**, 335–363.

Pier, B. 2002 On the frequency selection of finite-amplitude vortex shedding in the cylinder wake. *J. Fluid Mech.* **458**, 407–417.

Pierrehumbert, R. 1984 Local and global baroclinic instability of zonally varying flow. *J. Atmos. Sci.* **41**, 2141–2162.

Protas, B. 2000 Analyse et contrôle des forces hydrodynamiques d'un écoulement bidimentionnel derrière un obstacle en mouvement. Application de la méthode du vortex. PhD Thesis, Warsaw University of Technologiy, Poland, and Université Paris VI. Paris, France.

Protas, B. & Wesfreid, J. E. 2002 Drag force in the open-loop control of the cylinder wake in the laminar regime. *Phys. Fluids* **14**, 810–826.

Protas, B. & Wesfreid, J. E. 2003 On the relation between the global modes and the spectra of drag and lift in periodic wake flows. *C. R. Méc.* **331**, 49–54.

Provansal, M., Mathis, C. & Boyer, L. 1987 Bénard-Von Karman instability: transient and forced regimes. *J. Fluid Mech.* **182**, 1–22.

Saffman, P. F. 1992 *Vortex Dynamics*. Cambridge University Press.

Schmid, P. J. & Henningson, D. S. 2001 *Stability and Transition in Shear Flows*. Springer.

Siggia, E. & Zippelius, A. 1981 Pattern selection in Rayleigh-Bénard convection. *Phys. Rev. Lett.* **47**, 835–838.

Thiria, B. 2005 Propriétés dynamiques et de stabilité dans les écoulements ouverts forcés. PhD Thesis, Université Paris VI. Paris, France.

Thiria, B., Bouchet, G. & Wesfreid, J. E. 2007*a* On the relation between linear stability analysis and mean flow properties in wakes. *Phys. Fluids* (submitted).

Thiria, B., Bouchet, G. & Wesfreid, J. E. 2007*b* Critical properties of forced wakes. *In preparation*.

Thiria, B., Goujon-Durand, S. & Wesfreid, J. E. 2006 Wake of a cylinder performing rotary oscillation. *J. Fluid Mech.* **560**, 123–147.

Triantafyllou, G., Triantafyllou, M. & Chryssostomidis, C. 1986 On the formation of vortex street behind stationary cylinder. *J. Fluid Mech.* **170**, 461–477.

Wesfreid, J. E., Goujon-Durand, S. & Zielinska, B. 1996 Global mode behavior of the streamwise velocity in wakes. *J. Phys. Paris* II **6**, 1343–1357.

Wesfreid, J. E., Pomeau, Y., Dubois, M., Normand, C. & Bergé, P. 1978 Critical effects in Rayleigh-Bénard convection. *J. Phys. Paris* **39**, 725–731.

Williamson, C. H. K. 1988 Defining a universal and continuous Strouhal-Reynolds number relationship for the laminar vortex shedding of a circular cylinder. *Phys. Fluids* **31**, 2742–2744.

Zielinska, B. J. A., Goujon-Durand, S., Dusek, J. & Wesfreid, J. E. 1997 Strongly nonlinear effect in unstable wakes. *Phys. Rev. Lett.* **79**, 3893–3896.

Zielinska, B. & Wesfreid, J. E. 1995 On the spatial structure of global modes in wake flow. *Phys. Fluids* **7**, 1418–1424.

Zippelius, A. & Siggia, E. 1983 Stability of finite amplitude convection. *Phys. Fluids* **26**, 2905–2915.